RESEARCH ARTICLE

# Preparation of modified biochar and its removal effect on triclosan (TCS) in water

Dingyu Ji[1], Xueming Li[1], Kaili Yang[1], Rui Wang[2], Yali Huang[3], Mingqing Chang[4, *]

[1]College of Resources and Environmental Engineering, Sichuan Water Conservancy Vocational College, Chongzhou, Sichuan, China. [2]China MCC5 Group Corp. Ltd., Chengdu, Sichuan, China. [3]Chengdu Society of Environmental Sciences, Chengdu, Sichuan, China. [4]Sichuan Academy of Environmental Policy and Planning, Chengdu, Sichuan, China.

**Received:** January 7, 2026; **accepted:** May 11, 2026.

**The residual chlorinated organic pollutants in water pose a threat to ecosystems and public health, making the development of efficient and advanced treatment technologies crucial. This study prepared a modified biochar-supported iron/palladium (Fe/Pd) nanoparticle composite material for activating sodium persulfate ($Na_2S_2O_8$) to enhance the removal of tetrachlorosilane (TCS) from water. A series of biochar were prepared through pyrolysis and chemical modifications with $HNO_3$, $H_2O_2$, $KMnO_4$, NaOH, HCl, HF. BC700-nZVI-Pd composite materials were then synthesized using these biochars as carriers. The composite materials were utilized to activate $Na_2S_2O_8$ to generate sulfate radicals ($SO_4\bullet^-$) for the degradation of TCS. The effects of persulfate concentration, initial TCS concentration, and solution pH on the removal efficiency were systematically investigated. The results showed that, under the conditions of $Na_2S_2O_8$ concentration of 1 mM, initial TCS concentration of 10 mg/L, and pH of 4, the removal rate of TCS reached 69.93% after 60 minutes of reaction. Mechanism analysis indicated that the synergistic effect of Fe/Pd nanoparticles and biochar effectively promoted the generation of $SO_4\bullet^-$, thereby achieving efficient oxidative degradation of TCS. This study provided a promising catalytic-oxidative synergistic system for the advanced removal of TCS from water.**

**Keywords:** modified biochar; triclosan; water pollution; industrial wastewater.

[*]**Corresponding author:** Mingqing Chang, Sichuan Academy of Environmental Policy and Planning, Chengdu, Sichuan 610041, China. Email: cmqingcd@126.com.

## Introduction

Water pollution is an urgent environmental problem. At present, more than 400 million people around the world are facing severe water shortages, and water pollution has aggravated the trend of water shortages and threatened public health. In recent years, chlorinated organic pollutants (COCs) have been continuously detected in water environment. Most chlorine-containing organic compounds have three effects on organisms, and long-term presence in the environment is harmful to ecosystems, so it has attracted global attention [1]. Triclosan (TCS) is a chlorinated phenolic compound widely used as an insecticide and is found in a variety of personal care products including hand sanitizers, mouthwashes, toothpastes, detergents, and cosmetics. The concentration of TCS in personal care products is as high as 0.3% [2]. TCS is very easy to cause water pollution and has adverse effects on the survival of organisms, while human

health problems will also arise when using water contaminated by TCS. Therefore, it is necessary to use reliable methods to remove TCS from water and improve the water purification effect [3]. Conventional treatment methods cannot completely remove TCS. The residual TCS will enter the surface water with the effluent [4]. According to the existing records, the highest concentrations in influent wastewater of wastewater treatment plants, wastewater, drinking water, sludge and biosolids are as high as 86,200 mg/L, 5370 mg/L, 103 mg/L, and 30 mg/kg, respectively [5]. TCS has a long half-life, and one of its remarkable features is its relatively high octanol water partition coefficient, which is conducive to its bioaccumulation. When TCS is directly photolyzed, it produces highly toxic dioxins, which are more harmful to the environment than TCS [6]. Therefore, to ensure the safety of groundwater environment, it is necessary to prepare remediation materials with high degradation, dichlorination, and detoxification ability.

Many TCS removal methods have been developed and applied, which can be divided into adsorption, redox, and biodegradation methods. In the adsorption method, solid adsorption can affect the transport of organic matter in the environment and requires neither high cost and energy nor high technical operation. The strong hydrophobicity of TCS has attracted much attention for its adsorption removal. In recent studies, adsorbents such as biochar, montmorillonite, activated carbon, carbon nanotubes, graphene, *etc*. have been used for adsorptive removal of TCS [7]. Vidovix *et al*. showed that adsorbents with larger pore volume were more effective in adsorption, and their width was about 1.3 - 1.8 times the kinetic diameter of target pollutants [8]. With the increase of the pH value of the solution, the TCS in the form of negative ions increases. Almeida-Naranjo *et al*. synthesized hydrotalcite using co-precipitation method [9]. Bano *et al*. prepared wastewater biochar and found that, under acidic conditions, the adsorption capacity of TCS by biochar was the largest [10]. Due to the wide distribution of TCS in soil, the removal of TCS in soil is also a current hotspot. Researchers determined the adsorption of TCS in wastewater-irrigated soil and studied the adsorption behavior of microplastics on TCS in soil [11, 12]. For redox method, the oxidation by-products can completely mineralize TCS through free radical oxidation reaction in the case of sufficient free radicals [13]. The presence of $CO_3^{2-}$ and $HCO_3^-$ in solutions can effectively scavenge ·OH radicals, resulting in a slow generation rate of ·OH and a decrease in TCS removal. Improving the ·OH radical generation ability of Fenton and Fenton-like systems is expected to improve the degradation ability of TCS [14]. In addition, the selection of catalyst has a decisive influence on the degradation effect of TCS. Under the same experimental conditions, its removal rate was enhanced compared to the conventional Fenton method, indicating the efficient catalytic ability of nanoscale zero-valent iron. It has been reported that nanoscale $BiFeO_3$ could effectively decompose $H_2O_2$ into ·OH radicals without light irradiation, and the presence of $H_2O_2$ effectively degraded organic pollutants in a wide pH range [15]. The biodegradation and removal effects of algae on TCS is more worthy of being studied. Cho *et al*. found that, when the mortality rate of microalgae was 50%, the effective concentration of TCS was $8 \times 10^3$ μg/L. Among them, the degradation of TCS by microalgae was the main removal mechanism, rather than adsorption, which suggested that microorganisms played an important role in the process of biodegradation of TCS [16]. In addition, studies have found that TCS can be largely removed in activated sludge systems with biodegradation being the main removal mechanism [17]. Through the analysis of sewage sludge, researchers found that the *Providenciarettgeri* MB-IIT strain was active and grew at higher TCS concentrations by using TCS as carbon and energy sources [18]. However, there are fewer microorganisms that degrade TCS under natural conditions, and the tolerance of microorganisms to TCS is also different [19]. The domesticated bacteria can survive in the high TCS range, have tolerance to the toxicity of TCS, and can remove TCS in a targeted manner such as

*Pseudomonas putida* and *Alkalinobacter xylose* oxidans [20]. Special attention should be paid to pH value and temperature during the treatment of TCS by biodegradation method [21].

Despite the existence of various methods, developing a material and technology that can efficiently, rapidly, and thoroughly degrade TCS in water with easy application remains a key issue that urgently needs to be addressed in the current field of water treatment. Conventional treatment methods often struggle to balance efficiency, cost, and deep purification requirements. This research prepared an efficient modified biochar-supported Fe/Pd nanoparticle composite material and established an enhanced removal system through the synergistic adsorption, reduction, and advanced oxidation by activating sodium persulfate to generate sulfate radicals. Biochar was treated with various chemical modifiers to systematically characterize its physicochemical properties. Fe/Pd nanoparticles were loaded to prepare the composite material. The research investigated the properties and influencing factors of the composite in the process of activated sodium persulfate to degrade TCS and explored its reaction mechanism. This study not only provided promising new material and method for the deep removal of TCS in water but also offered experimental evidence for understanding the degradation mechanism of biochar-based composite materials synergistically activating persulfate, which held positive significance for ensuring water environmental safety and public health.

## Materials and methods

### Preparation of biochar and modified biochar

10.00 grams of rice straw powder obtained from a local farm in Chongzhou, Sichuan, China was compacted in OTF-1200X crucible (Kejing Material Technology Co., Ltd., Hefei, Anhui, China). Under the protection of a high-purity nitrogen atmosphere with the flow rate controlled at 200 mL/min, the temperature was raised at a rate of 5°C/min to the target pyrolysis temperatures of 300°C, 500°C, or 700°C and maintained for 2 hours. The obtained biochar was ground, sieved through a 100-mesh sieve, and stored in a desiccator for future use. The biochar samples pyrolyzed at 300°C, 500°C, and 700°C were designated as BC300, BC500, and BC700, respectively. For chemical modification, 10 g of each biochar (BC300, BC500, or BC700) was placed in 200 mL of 1 mol/L $HNO_3$, $H_2O_2$, $KMnO_4$, NaOH, HCl, or HF solutions, respectively. The mixtures were oscillated on ZQLY-180 thermostatic shaking incubator (Shanghai Zhichu Instrument Co., Ltd., Shanghai, China) at 25°C and 150 rpm for 24 h. The mixture was repeatedly rinsed and filtered with distilled water until the pH of the filtrates stabilized before being dried at 80°C, ground through a 100-mesh sieve, and stored for later use. The chemically modified samples were denoted as XBCY, where X represented the modifying agents with N for $HNO_3$, P for $H_2O_2$, M for $KMnO_4$, S for NaOH, C for HCl, F for HF, while Y represented the pyrolysis temperature.

### Synthesis of BC700-nZVI-Pd composite material

2 g of $FeSO_4 \cdot 7H_2O$ and 100 mg of modified biochar (BC700) were dispersed in 100 mL of deoxygenated water. After shaking at 25°C and 150 rpm for 24 h, 100 mL of anhydrous ethanol was added. The entire mixture was transferred to a 500 mL three-necked flask and deoxygenated with nitrogen and stirred for 15 minutes to achieve homogeneity. Under vigorous stirring, 200 mL of a freshly prepared 0.5 mol/L $KBH_4$ solution with 4 drops of 0.5 mol/L NaOH being added for stabilization was slowly added dropwise to the mixed solution, and the reaction was continued for 60 minutes to form black particles (nZVI). The resultant black nZVI particles were separated from the liquid phase by magnetic separation using a N52 grade, 50 mm × 25 mm × 10 mm rectangular neodymium magnet (Ningbo Strong Magnet Co., Ltd., Ningbo, Zhejiang, China) against the outer wall of the flask. The magnetic separation was performed for approximately 2 - 3 minutes under the continuous protection of the nitrogen

atmosphere to prevent oxidation. The clear supernatant was carefully decanted, and the magnetically held solids were collected. The product was first washed three times with deoxygenated deionized water to remove excess $KBH_4$ followed by three washes with ethanol. The entire reaction was conducted under a nitrogen environment to prevent oxidation. After separating the biochar-loaded $Fe^o$ particles, 12.657 mg of palladium acetate particles (Pd/Fe = 1.5% wt) was dissolved in 20 mL of ethanol and added to the sample bottle containing the biochar-loaded $Fe^o$ particles. After ultrasonication for 10 minutes at 25°C and 45 kHz, magnetic separation was performed again using the same neodymium magnet under ambient conditions to collect the final composite. The final particles (BC700-nZVI-Pd) were dried at 60°C in DZF-6020 vacuum drying oven (Shanghai Yiheng Scientific Instrument Co., Ltd., Shanghai, China), ground through a 100-mesh sieve, and stored in a vacuum desiccator.

**Characterization of biochar**

The specific surface areas and pore structures of the biochar were determined by $N_2$ adsorption-desorption at 77 K using a Micromeritics ASAP 2460 analyzer (Micromeritics Instrument Corporation, Norcross, GA, USA). The biochar samples were vacuum degassed at 105°C for 16 hours before the analysis. The specific surface area of the sample was calculated using the Brunauer-Emmett-Teller (BET) method based on adsorption data within the relative pressure range of 0.05 to 0.30 ($P/P_o$). The ash content was obtained by combusting the biochar in a muffle furnace at 800°C for 4 hours. The organic C, H, N, and S contents of the biochar were determined by using an Elementar Vario EL III elemental analyzer (Elementar Analysensysteme GmbH, Langenselbold, Germany) with two parallel measurements to calculate the O content as follows.

$$O\% = 100\% - \left(C\% + H\% + N\% + S\% + ash\%\right) \quad (1)$$

The pore volume and pore size distribution were determined by analyzing the desorption curve data using the Barrett-Joyner-Halenda (BJH) model.

**TCS degradation**

A 1,000 mg/L TCS stock solution was prepared using methanol as the solvent and stored in a brown bottle at 4°C in the dark. The stock solution was diluted with ultrapure water to the desired initial concentrations of 5, 10, 15, 20 mg/L, respectively, ensuring the methanol volume fraction was less than 0.1% (v/v). All batch degradation experiments were conducted in HZQ-F160 constant temperature oscillating shaker (Dongming Medical Instrument Factory, Xuzhou, Jiangsu, China) at 25°C and 150 rpm. 20.0 mL of 10 mg/L TCS solution was added to a 50 mL capped Erlenmeyer flask followed by adding BC700-nZVI-Pd composite material at a solid-liquid ratio of 0.16 g/L, i.e. 3.2 mg in 20 mL solution. 200 µL of a freshly prepared 0.1 M $Na_2S_2O_8$ solution was immediately added to achieve a final concentration of 1 mM, thereby initiating the reaction (t = 0). To study the effects of key parameters, the following conditions were varied with $Na_2S_2O_8$ concentrations of 0.0, 0.2, 0.4, 0.8, 1.0 mM in $[TCS]_o$ = 10 mg/L, initial TCS concentration of 5, 10, 15 mg/L in $[Na_2S_2O_8]_o$ = 1 mM, initial pH at 4, 5, 7, 9 adjusted with 0.1 M $HNO_3$ or NaOH in $[TCS]_o$ = 10 mg/L and $[Na_2S_2O_8]_o$ = 1 mM. To distinguish reduction from oxidation, 0.16 g/L BC700-nZVI-Pd was mixed with 20 mg/L TCS for 24 h followed by adding $Na_2S_2O_8$ to a final concentration of 1 mM to initiate the oxidation phase. 2.0 mL aliquots were taken at predetermined time intervals and quenched immediately with 0.2 mL of absolute ethanol. After filtering through 0.45 µm nylon membranes, the residual TCS concentration was analyzed by using Agilent 1260 Infinity II high-performance liquid chromatography (HPLC) (Agilent Technologies, Santa Clara, CA, USA) equipped with a ZORBAX Eclipse Plus C18 column (4.6 mm × 150 mm, 5 µm). The mobile phase was methanol/0.1% formic acid in water at a ratio of 85:15 (v/v) at a flow rate of 1.0 mL/min. The column temperature was at 30°C with the

detection wavelength of 280 nm and injection volume of 20 µL. The removal efficiency (η) was calculated as follows.

$$\eta(\%) = (1 - C_t / C_0) \times 100\% \quad (2)$$

where $C_0$ and $C_t$ were the initial concentration of TCS and the residual concentration at time t, respectively. The control experiments were conducted to investigate the role of each component, which included 20 mL of 10 mg/L TCS alone, 20 mL of 10 mg/L TCS + 3.2 mg BC700, 20 mL of 10 mg/L TCS + 1 mM $Na_2S_2O_8$, 20 mL of 10 mg/L TCS + 3.2 mg BC700-nZVI-Pd. All control experiments followed the same procedures and sampled at 60 minutes.

**Statistical analysis**

All experiments were performed in triplicate. Data were presented as mean ± standard deviation (SD). SPSS Version 26.0 (IBM, Armonk, NY, USA) was employed for statistical analysis. One-way analysis of variance (ANOVA) followed by Tukey's post-hoc test were performed to assess statistical significance. *P* value less than 0.05 was considered statistically significant.

## Results and discussion

**Characterization analysis**

The elemental analysis of unmodified and modified biochar demonstrated that, for the same modified biochar, with the increase of pyrolysis temperature, the C content gradually increased due to the accumulation of fixed carbon, while the removal of $H_2O$, hydrocarbons, $H_2$, *etc*. during the carbonization process led to the gradual decrease of H and O contents. The H/C ratio decreased with the increase of pyrolysis temperature and the H/C of BC300, BC500, and BC700 were 0.88, 0.56, and 0.41, respectively, indicating that the aromaticity of biochar increased with the increase of pyrolysis temperature. The (0 + N)/C ratio of biochar treated with HF was the lowest, and the (O+N)/C ratio of FBC700 was 0.03, which was much smaller than the (O + N)/C ratio of BC700 of 0.35, indicating that the hydrophobicity of FBC700 was significantly enhanced. The ash content of the modified biochar was reduced, among which the ash content of the HF-modified biochar was reduced the most. The ash contents of FBC300, FBC500, and FBC700 were 0.92%, 2.79%, and 19.14%, respectively, which was about 20% lower than that of unmodified biochar (Table 1). The results suggested that HF modification had a greater effect on the elemental composition and ash content of biochar than other modifications. The specific surface area and total pore volume of unmodified and modified biochar showed that, for the same modified biochar, when the pyrolysis temperature of biochar was between 300 - 800°C, the increase of pyrolysis temperature caused the micropore wall to collapse and the micropore volume to decrease, but the total pore volume of biochar and specific surface area increased. Furthermore, the increase in temperature caused more volatile substances to be released from the biomass surface, resulting in char with more pores, which significantly increased the specific surface area of biochar. The specific surface areas of BC300, BC500, and BC700 were 2.51, 8.03 and 134.01 $m^2/g$, respectively. Among them, the specific surface area of biochar modified by HF increased the most significantly. The specific surface areas of FBC500 and FBC700 reached 159.38 and 388.89 $m^2/g$, respectively. The specific surface areas of SBC500 and SBC700 also reached 165.89 and 259.57 m/g (Table 2). The reason was that modifiers such as HF and NaOH removed ash and inorganic matter from the pore structure of biochar and removed some soluble impurities, thereby increasing the specific surface area and pore volume. The increase of the specific surface area of biochar was beneficial to the adsorption of TCS by the surface and pore structure of biochar. In addition, the developed pore structure of modified biochar was also beneficial to increasing the loading sites of iron-palladium nanoparticles. The degradation mechanism of TCS by modified biochar-loaded Fe/Pd nanoparticles included the adsorption of biochar and the reduction of Fe/Pd nanoparticles. The

**Table 1.** Elemental analysis of biochar and modified biochar at different pyrolysis temperatures.

| Sample | Ash content | N (%) | C (%) | H (%) | S (%) | 0(%) | H/C | (O+N)/C |
|---|---|---|---|---|---|---|---|---|
| BC300 | 22.48 | 1.25 | 61.60 | 4.54 | 0.51 | 32.10 | 0.88 | 0.41 |
| CBC300 | 17.93 | 1.13 | 60.76 | 4.88 | 0.19 | 33.04 | 0.96 | 0.42 |
| FBC300 | 0.92 | 1.14 | 62.25 | 4.94 | 0.12 | 31.56 | 0.95 | 0.40 |
| SBC300 | 10.00 | 1.14 | 59.89 | 5.16 | 0.15 | 33.65 | 1.03 | 0.44 |
| PBC300 | 17.96 | 1.04 | 58.18 | 4.94 | 0.14 | 35.71 | 1.02 | 0.48 |
| NBC300 | 19.45 | 1.19 | 61.86 | 4.94 | 0.19 | 31.82 | 0.96 | 0.40 |
| KBC300 | 25.47 | 1.02 | 52.99 | 5.23 | 0.19 | 40.57 | 1.18 | 0.59 |
| BC500 | 35.26 | 1.12 | 67.21 | 3.11 | 0.58 | 27.98 | 0.56 | 0.33 |
| CBC500 | 27.57 | 1.15 | 69.00 | 3.17 | 0.22 | 26.46 | 0.55 | 0.30 |
| FBC500 | 2.79 | 1.28 | 76.60 | 3.24 | 0.16 | 18.73 | 0.51 | 0.20 |
| SBC500 | 10.67 | 1.16 | 70.69 | 3.36 | 0.18 | 24.61 | 0.57 | 0.28 |
| PBC500 | 29.09 | 1.13 | 72.38 | 3.47 | 0.23 | 22.79 | 0.58 | 0.25 |
| NBC500 | 26.68 | 1.75 | 64.91 | 3.10 | 0.18 | 30.06 | 0.57 | 0.37 |
| KBC500 | 35.33 | 0.93 | 57.53 | 3.77 | 0.19 | 37.58 | 0.79 | 0.50 |
| BC700 | 40.50 | 1.43 | 66.57 | 2.30 | 0.36 | 29.35 | 0.41 | 0.35 |
| CBC700 | 33.41 | 1.55 | 67.69 | 2.50 | 0.31 | 27.95 | 0.44 | 0.33 |
| FBC700 | 19.14 | 2.17 | 94.72 | 2.70 | 0.48 | 1.93 | 0.34 | 0.03 |
| SBC700 | 19.17 | 1.69 | 73.42 | 2.58 | 0.60 | 21.71 | 0.42 | 0.24 |
| PBC700 | 36.51 | 1.74 | 75.93 | 2.89 | 0.48 | 18.96 | 0.46 | 0.21 |
| NBC700 | 32.92 | 1.90 | 67.07 | 2.59 | 0.39 | 28.05 | 0.46 | 0.34 |
| KBC700 | 37.15 | 1.41 | 61.04 | 3.11 | 0.35 | 34.09 | 0.61 | 0.44 |

**Table 2.** BET analysis of biochar and modified biochar with different pyrolysis temperatures.

| Sample | Specific surface area ($m^2/g$) | Pore volume ($mm^3/g$) | Sample | Specific surface area ($m^2/g$) | Pore volume ($mm^3/g$) | Sample | Specific surface area ($m^2/g$) | Pore volume ($mm^3/g$) |
|---|---|---|---|---|---|---|---|---|
| BC300 | 2.51 | 4.39 | BC500 | 8.03 | 11.52 | BC700 | 134.04 | 83.12 |
| CBC300 | 2.45 | 3.60 | CBC500 | 62.71 | 44.38 | CBC700 | 189.98 | 85.14 |
| FBC300 | 5.68 | 9.66 | FBC500 | 159.38 | 142.81 | FBC700 | 388.89 | 331.70 |
| SBC300 | 2.95 | 4.14 | SBC500 | 165.89 | 122.21 | SBC700 | 259.57 | 214.14 |
| PBC300 | 2.48 | 3.75 | PBC500 | 38.25 | 30.35 | PBC700 | 87.38 | 76.90 |
| NBC300 | 1.34 | 1.45 | NBC500 | 25.44 | 19.46 | NBC700 | 214.69 | 129.17 |
| KBC300 | 23.19 | 22.71 | KBC500 | 103.38 | 94.79 | KBC700 | 243.42 | 200.09 |

final products of TCS degradation were mainly $CO_2$, $H_2O$, and small carboxylic acids molecule. In practical applications, some toxic compounds were still produced during the application process, polluting soil and groundwater, and causing harm to human health. Therefore, to completely degrade TCS, persulfate was added to the reaction system of modified biochar-loaded Fe/Pd nanoparticles with TCS, and advanced oxidation technology was used to degrade TCS. The biochar-loaded Fe/Pd nanoparticles and TCS almost reached equilibrium after 24 h of reaction. The results indicated that, in the absence of added $Na_2S_2O_8$, the removal rate of TCS by BC700-nZVI-Pd reached 19.38% after 24 hours of reaction. Given that $Cl^-$ ions could interfere with $Na_2S_2O_8$-mediated reactions, 10 mM $Cl^-$ was not introduced into the reaction system as a background electrolyte. Furthermore, as the initial concentration of TCS in the solution was increased from 10 mg/L to 20 mg/L, the removal rate of TCS by BC700-nZVI-Pd

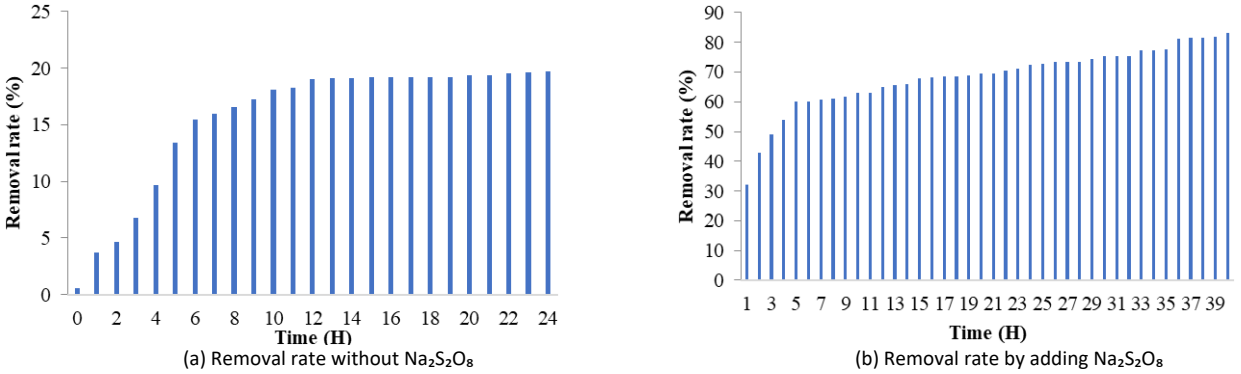


(a) Removal rate without $Na_2S_2O_8$ (b) Removal rate by adding $Na_2S_2O_8$

**Figure 1.** Effect of adding $Na_2S_2O_8$ on TCS degradation of composite materials.

consequently decreased. After adding $Na_2S_2O_8$, $SO_4\bullet^-$ was rapidly generated, which reacted with the remaining TCS to reduce the concentration of TCS in the solution. After adding $Na_2S_2O_8$ for 5 minutes, the removal rate of TCS increased from 19.38% to 60.18%. After adding $Na_2S_2O_8$ for 30 minutes and 40 minutes, the removal rates of TCS reached 80.20% and 82.26%, respectively, indicating that the reaction gradually tended to equilibrium (Figure 1). The results confirmed that Fe/Pd nanoparticles could effectively activate TCS in $Na_2S_2O_8$ degradation solution, and within 30 minutes of adding sodium persulfate, the removal rate of TCS reached 80%. Fe/Pd bimetallic nanoparticles could promote the decomposition of persulfate, produce more $SO_4\bullet^-$, and thus promote the oxidative removal of TCS. Since the adsorption and reduction of TCS by biochar-loaded Fe/Pd nanoparticles was first performed before $Na_2S_2O_8$ being added for oxidation reaction, the reaction time was still relatively long. The removal rate of TCS by adsorption and reduction was not high, and the purpose of rapid and efficient degradation of TCS could not be achieved. Therefore, $Na_2S_2O_8$ was directly added to the reaction system of biochar-loaded Fe/Pd nanoparticles and TCS to explore the effects of various factors on TCS removal.

**Effect of $Na_2S_2O_8$ concentration**

$Na_2S_2O_8$ was activated during the reaction to produce sulfate radicals $SO_4\bullet^-$, which were the main redox species for degrading TCS. The concentration of $Na_2S_2O_8$ in the reaction solution affected the removal rate of TCS in the reaction system of biochar-loaded Fe/Pd nanoparticles and TCS. The results showed that the reaction mainly occurred in the first 10 minutes. As the reaction proceeded, the reaction gradually reached equilibrium. In the reaction system without $Na_2S_2O_8$, after 60 minutes of reaction, the removal rate of TCS by BC700-nZVI-Pd was 26.44%. When $Na_2S_2O_8$ was added, the removal rate reached about 40% in the first 5 minutes of reaction. With the increase of the concentration of $Na_2S_2O_8$, the removal rate of TCS by BC700-nZVI-Pd gradually increased. When the concentration of persulfate was 1 mM, the removal rate of TCS by BC 700-nZVI-Pd was 69.93%. As the concentration of $Na_2S_2O_8$ increased, the amount of sulfate radical $SO_4\bullet^-$ in the solution that could be used to react with TCS increased, and the removal rate of TCS also increased. When the concentration of $Na_2S_2O_8$ was 1 mM, about 70% of TCS was removed. Therefore, the dosage of $Na_2S_2O_8$ in the reaction system was determined as 1 mM (Figure 2).

**Effect of TCS concentration**

The effect of the initial concentration of TCS on the degradation of TCS by biochar-loaded Fe/Pd nanoparticles demonstrated that, as the initial concentration of TCS increased, the removal rate of TCS gradually decreased, and the reaction rate gradually slowed down. When the concentrations of TCS were 5, 10, and 15 mg/L, respectively, the removal rates of TCS were 61.69%, 51.68%, and 41.16% after 60 minutes of

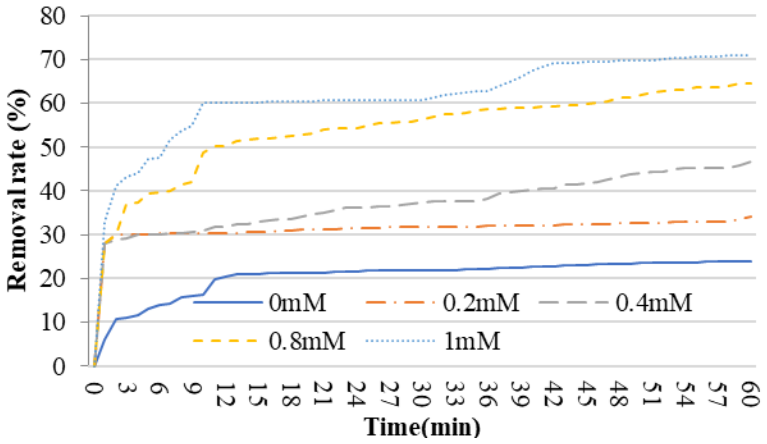


**Figure 2.** Effect of persulfate concentration on TCS degradation of composite materials.

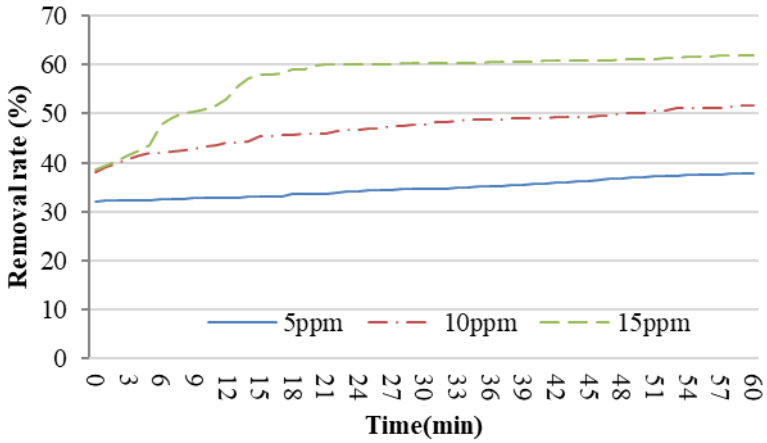


**Figure 3.** Effect of TCS concentration on TCS degradation of composite materials.

reaction. When the concentration of TCS was low, the added $Na_2S_2O_8$ could produce enough sulfate radicals $SO_4^{\bullet -}$ to degrade TCS. As the concentration of TCS increased, TCS and its degradation intermediates were adsorbed onto the surface of BC700-nZVI-Pd, which masked the adsorption sites on BC700-nZVI-Pd. The reaction between $Na_2S_2O_8$ and BC700-nZVI-Pd was limited, and $Na_2S_2O_8$ produced fewer active substances. When the concentration of TCS was low, there were enough free radicals in the reaction system to remove more TCS. Therefore, as the concentration of TCS in the reaction system increased, the removal rate of TCS decreased (Figure 3).

**Effect of pH**

As the pH increased, the removal rate of TCS decreased. When the pH of the solution increased from 4 to 9, the removal rate of TCS decreased from 67.06% to 40.23% (Figure 4). The results showed that, when the pH of the reaction system was acidic, it was conducive to the reaction. When the pH was low, it was conducive to the corrosion of $Fe^0$ and promoted the generation of $Fe^{2+}$. There were more $H^+$ in the solution, which reacted with the hydroxide deposited on the surface of $Fe^0$ and promoted the contact between $Fe^0$ and pollutants. In addition, some $Na_2S_2O_8$ reacted with $H^+$ to generate $SO_4^{\bullet -}$ free radicals, which promoted the reaction. When the pH gradually increased, the $H^+$ in the solution decreased. As the reaction proceeded, hydroxide precipitation was

generated on the surface of $Fe^0$ to further inhibit the reaction of $Fe^0$.

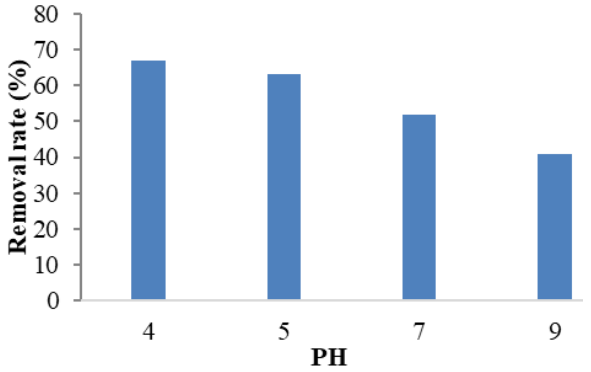


**Figure 4.** Effect of initial pH of solution on TCS degradation of composite materials.

**Mechanism analysis**

The hypothesized reaction mechanism for the model of BC700-nZVI-Pd activating $Na_2S_2O_8$ to degrade TCS showed that this model was inferred based on its excellent catalytic performance such as 80% removal rate within 30 minutes and experimental results such as pH effect. The core assumption was that Fe/Pd nanoparticles could be well dispersed on the biochar carrier, thereby exposing abundant active sites and achieving efficient electron transfer and catalytic cycling. However, this inference about the dispersion state of nanoparticles had not been directly confirmed by morphological characterization. The ideal dispersed state was a key prerequisite for its efficient catalytic performance, but this conclusion still needed to be verified. The change in pH value not only significantly affected the corrosion of $Fe^o$ and the activation of persulfate but also played a crucial role in the catalytic activity and stability of Pd component in Fe/Pd nanoparticles, which was the key to its superior performance compared to a single zero valent iron (nZVI) system. Under acidic conditions, sufficient $H^+$ in the solution could effectively inhibit the surface passivation of Pd active sites. Pd was easily covered by reaction intermediates or dissolved oxygen complexes during the reaction, and $H^+$ could protonate these substances, clean and expose the active surface of Pd, ensuring its continuous catalysis of the electron transfer between $Fe^{2+}$ and $S_2O_8^{2-}$ generated by $Fe^o$ corrosion, thereby promoting the continuous generation of $SO_4^{\bullet-}$. The reaction equation was expressed as follows.

Pd- surface + $2H^+ \rightarrow$ Pd surface (active) + $H_2$

In addition, the acidic environment inhibited the deposition of $Fe^o/Fe^+$ hydroxide on the surface of Pd, avoiding the blockage of Pd active sites and ensuring its efficient catalytic activity. On the contrary, under neutral and alkaline conditions, the surface of Pd was more prone to the formation of oxide or hydroxide layers, and the $Fe^{2+}$ generated by $Fe^o$ corrosion quickly transformed into $Fe(OH)_2$ or $Fe(OH)_3$ precipitates and covered the surface of Pd, seriously hindering its function as an electron mediator and leading to a sharp decrease in catalytic cycle efficiency. Therefore, maintaining an acidic environment was not only necessary for optimizing $Fe^o$ activation but also a prerequisite for maintaining high activity of Pd catalysts and preventing their deactivation, which was crucial for the efficient and sustainable operation of Fe/Pd bimetallic systems. This mechanism was reflected in the overall reactions, where, under acidic conditions, Pd could efficiently catalyze the transfer of electrons from $Fe^o$ to persulfate and promote the cycling of $Fe^{2+}/Fe^{3+}$, thereby significantly increasing free radical production and TCS degradation rate (Figure 5).

**Limitations and future research directions**

This study conducted a detailed characterization of various chemically modified biochar. The results showed that the modification significantly improved the specific surface area and hydrophobicity of the materials. However, in the subsequent construction of the catalytic system, this study chose unmodified BC700 as the matrix for loading Fe/Pd nanoparticles mainly based on the two in-depth considerations including the transformation of the core objective of the experiment and the key factor in carrier selection. The initial modification aimed to

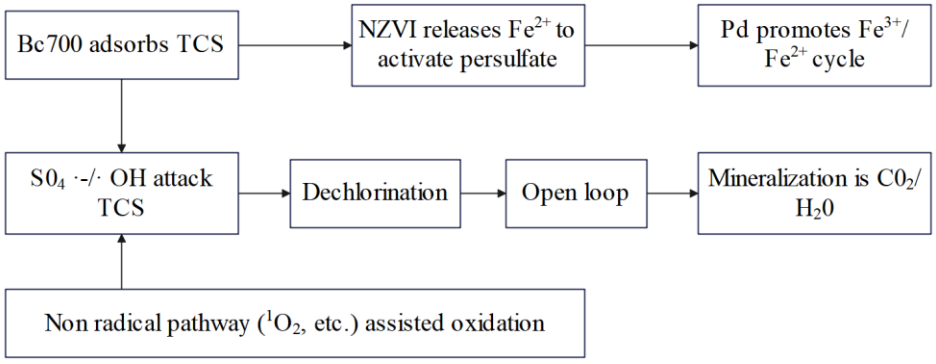


**Figure 5.** Reaction mechanism of BC700-nZVI-Pd and persulfate for TCS degradation.

optimize the adsorption performance of biochar, while the core of subsequent experiments was to investigate its catalytic activation of $Na_2S_2O_8$. Characterization revealed that, while strong acid/strong base modification increased the specific surface area, it might also etch or destroy some aromatic structures and key functional groups on the surface of biochar, which were crucial for electron transfer, stable loading of nano zero valent iron (nZVI), and activation of persulfate. Although unmodified BC700 had a lower specific surface area, its surface chemical environment might be more favorable for the adhesion and catalytic cycling of $Fe^0$ and $Pd^0$. An ideal catalytic carrier required a balance between specific surface area and surface chemical properties. Preliminary experiments showed that, although FBC700 had stronger adsorption capacity, BC700-nZVI-Pd composite material exhibited higher catalytic activity in the system of activating $Na_2S_2O_8$ to degrade TCS, which suggested that, for this catalytic reaction, the conductivity and surface functional group properties of biochar were more important than simply physical adsorption sites. Therefore, to focus on the exploration of catalytic mechanisms, this study selected BC700 as a representative carrier for further comprehensive research. A major limitation of this study was the insufficient characterization of the microstructure of composite materials. Although the excellent catalytic activity of BC700-nZVI-Pd had been indirectly demonstrated through degradation experiments, there was a lack of direct microscopic image evidence to observe and confirm the actual loading, dispersion, particle size distribution, and element distribution of Fe/Pd nanoparticles on the surface of biochar. Therefore, the potential mechanism of the "absence of aggregation" of nanoparticles was an idealized model derived from the performance observations.

## Conclusion

This research proposed a BC700-nZVI-Pd activating $Na_2S_2O_8$ system for TCS degradation, investigated the concentration of $Na_2S_2O_8$ and the initial concentration of TCS, and explored the reaction mechanism of the reaction system. The results showed that, when the concentration of $Na_2S_2O_8$ was 0 to 1 mM, the removal rate of TCS increased with the increase of $Na_2S_2O_8$ concentration. When the concentration of TCS in the solution was 5 to 15 mg/L, the removal rate decreased with the increase of TCS concentration. When the initial pH of the solution was 4, it was conducive to the reaction. Moreover, the higher the pH, the lower the removal rate. The reaction mechanism mainly included $Fe^{2+}$ generated by $Fe^0$ corrosion and C-OH on biochar, which activated $Na_2S_2O_8$ to generate sulfate radicals $SO_4\bullet^-$ to degrade TCS. Under the synergistic effect of biochar and Fe/Pd nanoparticles, the production of $SO_4\bullet^-$ was promoted, thereby promoting the degradation of TCS. This research explored the removal effect of

TCS in water through laboratory research. However, it had not yet been applied in practice. It is necessary to verify the effect of this method in practice and the practicality from a cost perspective, which is also the direction of subsequent research.

## Acknowledgements

This study was supported by Sichuan Provincial Department of Water Resources Research Project (Grant No. SKY2019-05).

## References

1. Wang J, Man H, Sun L, Zang S. 2022. Carbon black: A good adsorbent for triclosan removal from water. Water. 14(4):576.
2. Nawong S. 2024. Pulsed-bed column adsorption for triclosan removal using macadamia nutshell activated carbon. Civ Eng J. 10(5):1645-1661.
3. Almeida-Naranjo CE, Frutos M, Guerrero VH, Villamar-Ayala CA. 2024. Characterization and performance of peanut shells in caffeine and triclosan removal in batch and fixed-bed column tests. Molecules. 29(12):2923.
4. Dai Q, Liu Z, Li H, Zhang R, Cai T, Yin J, *et al*. 2024. Enhanced dewaterability and triclosan removal of waste activated sludge with iron-rich mineral-activated peroxymonosulfate. Waste Manag. 182(1):271-283.
5. Jabłońska-Trypuć A. 2023. A review on triclosan in wastewater: Mechanism of action, resistance phenomenon, environmental risks, and sustainable removal techniques. Water Environ Res. 95(9):e10920.
6. Cho EJ, Kang JK, Moon JK, Um BH, Lee CG, Jeong S, *et al*. 2021. Removal of triclosan from aqueous solution via adsorption by kenaf-derived biochar: Its adsorption mechanism study *via* spectroscopic and experimental approaches. J Environ Chem Eng. 9(6):106343.
7. Ali I, Imanova GT, Albishri HM, Alshitari WH, Locatelli M, Siddiqui MN, *et al*. 2022. An ionic-liquid-imprinted nanocomposite adsorbent: simulation, kinetics and thermodynamic studies of triclosan endocrine disturbing water contaminant removal. Molecules. 27(17):5358.
8. Vidovix TB, Januário EFD, Araujo MF, Bergamasco R, Vieira AMS. 2022. Investigation of two new low-cost adsorbents functionalized with magnetic nanoparticles for the efficient removal of triclosan and a synthetic mixture. Environ Sci Pollut Res. 29:46813-46829.
9. Almeida-Naranjo CE, Cuestas J, Guerrero VH, Villamar-Ayala CA. 2024. Efficient decontamination: Caffeine/triclosan removal using rice husk in batch and fixed-bed columns. Water. 16(2):197.
10. Bano F, Malik A, Ahammad SZ. 2021. Removal of estradiol, diclofenac, and triclosan by naturally occurring microalgal consortium obtained from wastewater. Sustainability. 13(14):7690.
11. Tian L, Sun H, Dong X, Wang J, Huang Y, Sun S. 2022. Effects of swine wastewater irrigation on soil properties and accumulation of heavy metals and antibiotics. J Soils Sediments. 22(3):889-904.
12. Cortés-Arriagada D, Ortega DE. 2023. Interaction mechanism of triclosan on pristine microplastics. Sci Total Environ. 891:164470.
13. Atengueno-Reyes K, Velasquez-Orta SB, Yanez-Noguez I, Monje-Ramirez I, Mijaylova-Nacheva P, Chavez-Mejia A, *et al*. 2023. Microalgal consortium tolerance to bisphenol A and triclosan in wastewater and their effects on growth, biomolecule content and nutrient removal. Ecotoxicol Environ Saf. 262:115117.
14. Li Y, Gong F, Yang W, Liu B. 2023. Effective triclosan removal by using porous aromatic frameworks in continuous fixed-bed column studies. Environ Sci Pollut Res. 30(57):121007-121013.
15. Jagini S, Thadurai S, Konda S, Saranga VK, Dheeravath B, Vurimindi H. 2021. Emerging contaminant (triclosan) removal by adsorption and oxidation process: comparative study. Model Earth Syst Environ. 7(2):2431-2438.
16. Cho EJ, Moon JK, Lee CG, Park SJ. 2022. Removal of triclosan from aqueous solution using biochar derived from seed shell of aesculus turbinata. Desalin Water Treat. 266(1):256-267.
17. Bayode AA, Akpotu SO, Omorogie MO, Vieira EM, Unuabonah EI. 2024. Self-assembly of ZnO-biochar/kaolinite/chitosan/GO with 1D/2D/3D heterojunctions for enhanced removal of estrogens and triclosan in water. BMC Chem. 18(1):243-255.
18. Navrozidou E, Remmas N, Melidis P, Sylaios G, Ntougias S. 2023. Biotreatment efficiency, degradation mechanism and bacterial community structure in an immobilized cell bioreactor treating triclosan-rich wastewater. Environ Technol. 44(10):1518-1529.
19. Franzoni RM, Bernardelli JKB, Silveira DD, Gomes SD, Lapolli FR, Carvalho KQD, *et al*. 2024. Performance of an anaerobic-oxic-anoxic (AOA) system in the simultaneous removal of nutrients and triclosan and bacterial community. Environ Technol. 45(3):544-558.
20. Gonzalez-Fernandez LA, Medellin-Castillo NA, Ocampo-Pérez R, Hernandez-Mendoza H, Berber-Mendoza MS, Aldama-Aguilera C. 2021. Equilibrium and kinetic modelling of triclosan adsorption on single-walled carbon nanotubes. J Environ Chem Eng. 9(6):106382.
21. Proenca BDSG, de Souza Antonio R, Cusioli LF, Vieira MF, Bergamasco R, Vieira AMS. 2023. Assessment of the natural zeolite adsorption capacity for the removal of triclosan from the aqueous medium. Desalin Water Treat. 292:165-175.